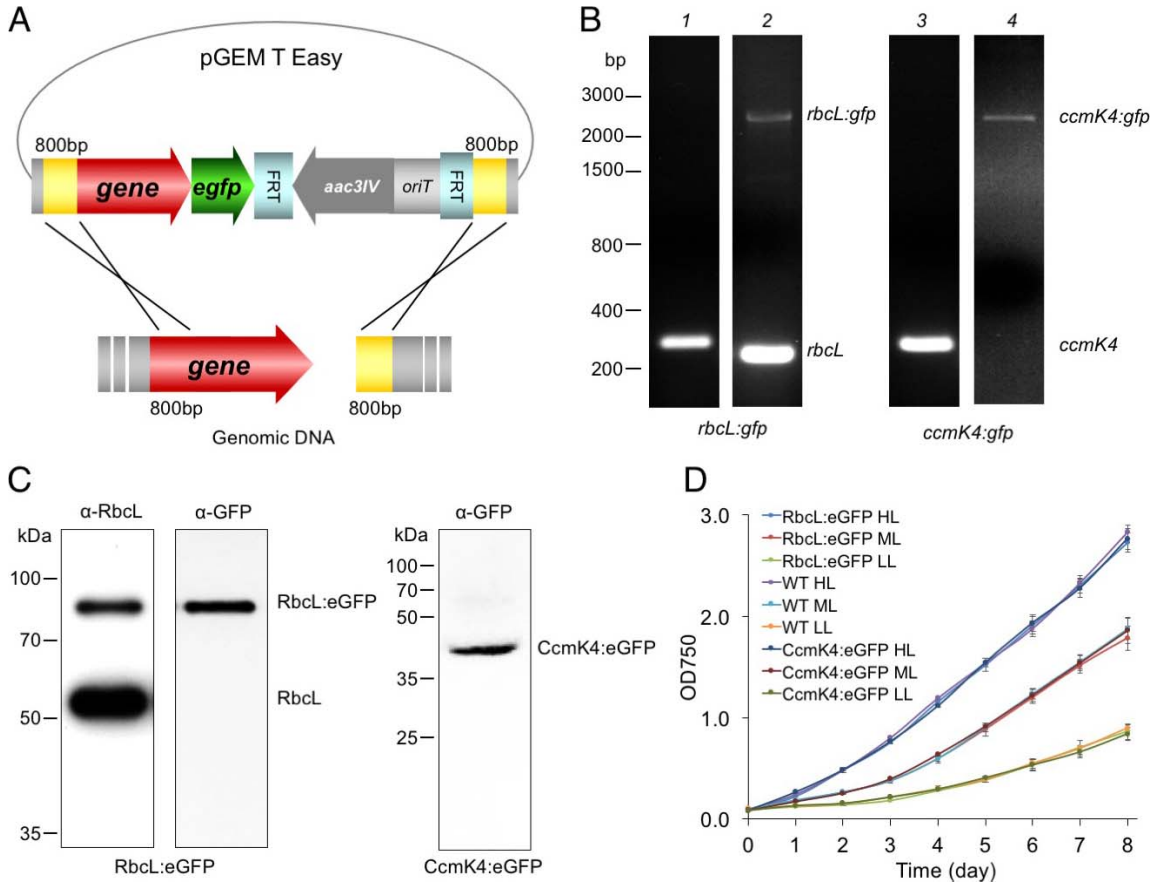

Supplemental Figure S1. Construction and characterization of RbcL:eGFP and CcmK4:eGFP *Synechococcus* strains. A, Strategy of eGFP fusion using REDIRECT protocol. B, PCR evaluation of RbcL:eGFP and CcmK4:eGFP genome. Lane 1 shows the *gfp* cassette fragment is fused to the C-terminus of *rbcL* in the RbcL:eGFP genome using the primers FRbcL-GFP_seg and GFP_rev (Supplemental Table S1). Lane 2 exhibits the *gfp* cassette fragment is partially segregated into the RbcL:eGFP genome. Lane 3 depicts the *gfp* cassette fragment is fused to the C-terminus of *ccmK4* in the CcmK4:eGFP genome using the primers FCcmK4-GFP_seg and GFP_rev (Supplemental Table S1). Lane 4 illustrates the *gfp* cassette fragment is fully segregated into the CcmK4:eGFP genome. C, Immunoblot analysis with anti-RbcL and anti-GFP antibodies of soluble fractions of the RbcL:eGFP strain and anti-GFP antibodies of soluble fractions of the CcmK4:eGFP strain, based on SDS-PAGE. Left, the band at around 83 kDa is consistent with the fusion of RbcL and eGFP, while 55 kDa refers to RbcL only. Protein quantification shows the RbcL:eGFP band is around 30% of the intensity of unfused RbcL band. Right, the 39 kDa band shows the fusion of CcmK4 and eGFP. D, Growth of wild-type, RbcL:eGFP and CcmK4:eGFP *Synechococcus* strains under HL, ML and LL. The growth curves monitored at OD 750nm demonstrated no significant change of the cell growth caused by GFP fusion. Cells were collected under log phase growth for imaging and analysis. Results are a mean ± SD of three independent cultures.

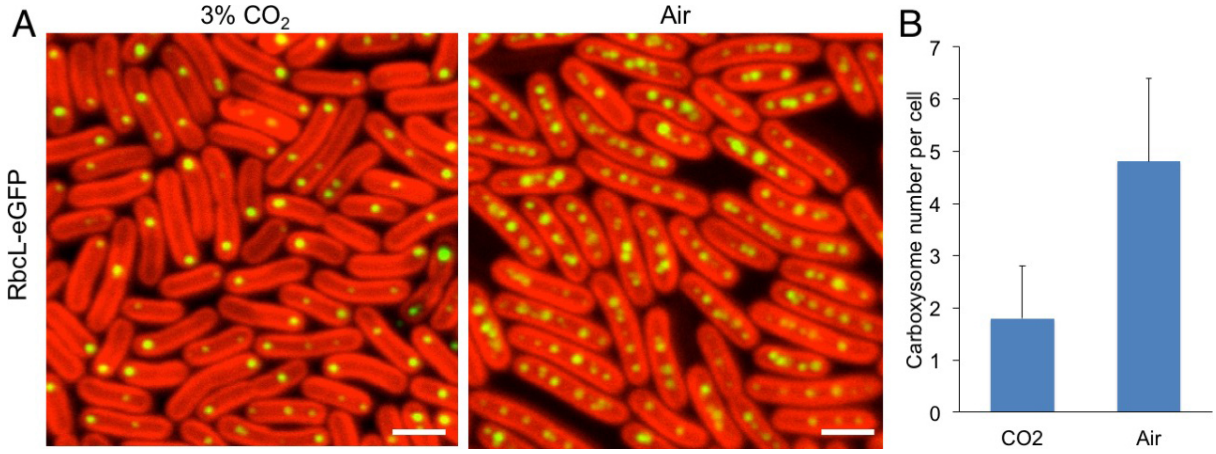

Supplemental Figure S2. Regulation of carboxysome biosynthesis in *Synechococcus* by CO_2. A, Confocal images of RbcL:eGFP strain confirms that 3% CO_2 suppresses the biosynthesis of carboxysomes relative to air. Scale bar: 2 μm. B, Average number of carboxysomes per cell in 3% CO_2 is lower than that in air ($P < 0.05$, $n = 100$). Error bars represent SD.

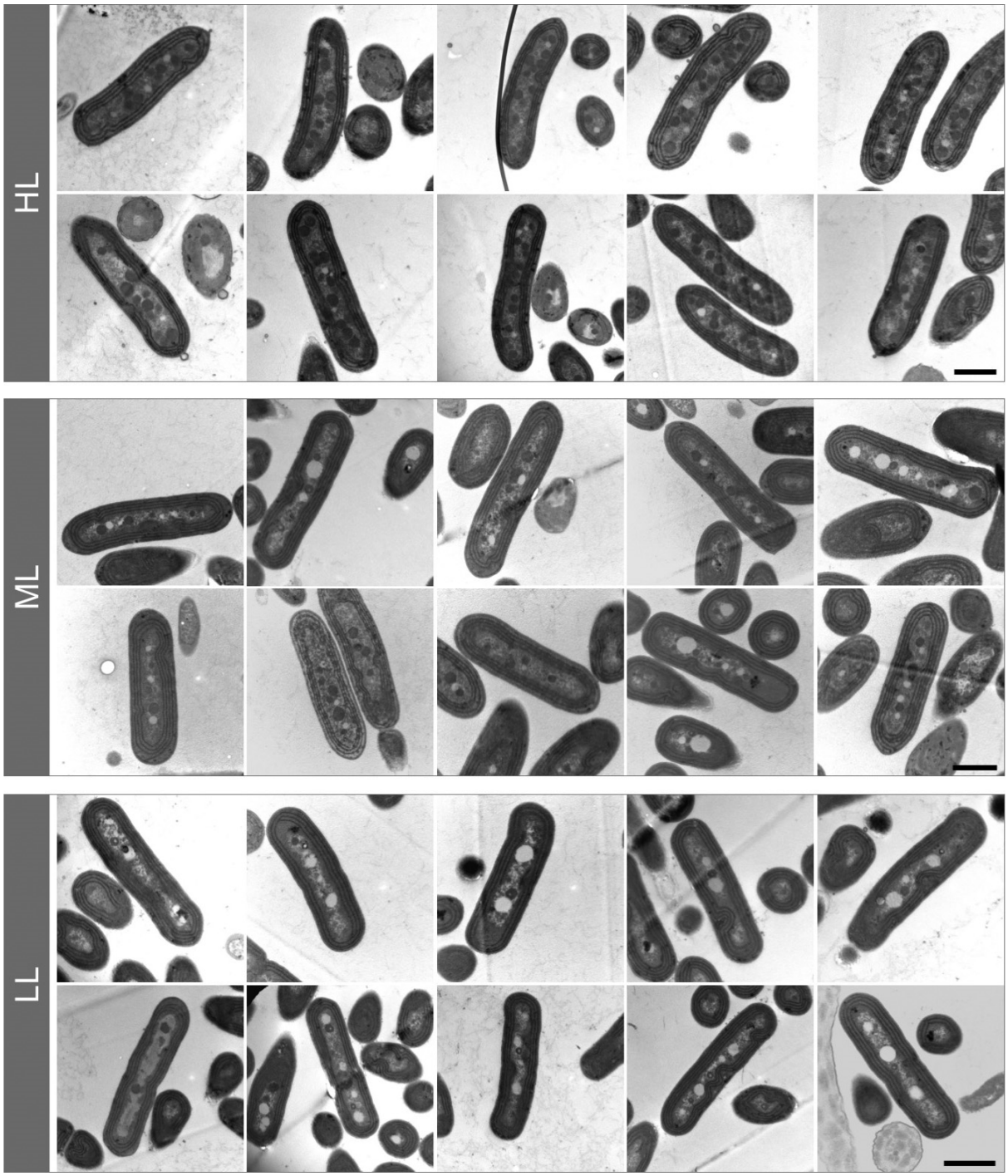

Supplemental Figure S3. Thin-section transmission electron microscopy images of wild-type *Synechococcus* cells grown under HL, ML and LL. The average numbers of carboxysomes per cell are 10.2 ± 2.0, 3.9 ± 0.8 and 1.6 ± 0.7, respectively (± SD, n = 30 for each light condition). Scale bar: 1 μm.

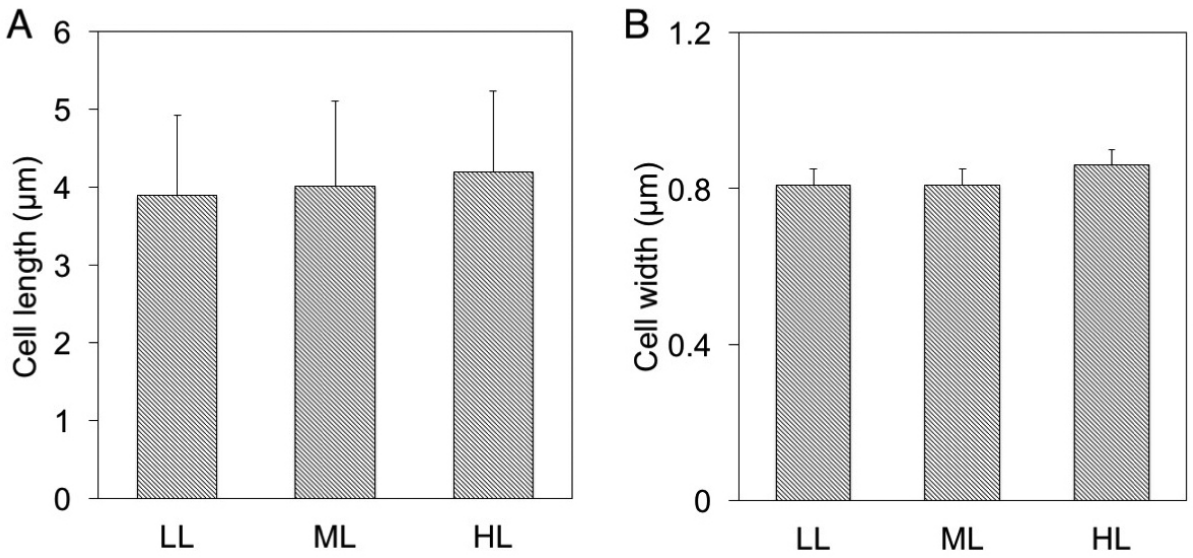

Supplemental Figure S4. The sizes of *Synechococcus* cells remain similar under the variation of light intensity. A, Averaged cell lengths are similar in LL, ML and HL ($P > 0.05$, $n = 500$). B, Difference in the averaged cell widths is not detectable in LL, ML and HL ($P > 0.05$, $n = 500$). Error bars represent SD.

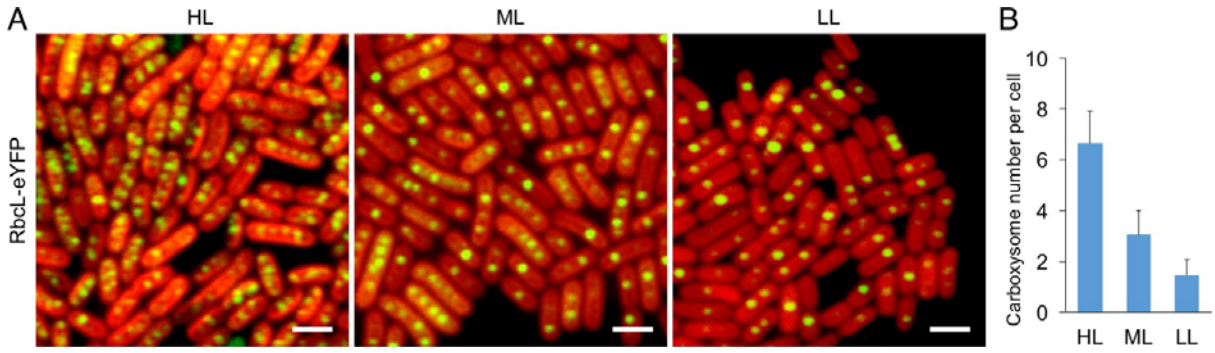

Supplemental Figure S5. Light regulation of carboxysome content in RbcL:YFP cells. A, Confocal microscopy images of the RbcL:YFP *Synechococcus* construct (pDFS621, PapcA:rbcL:YFP, Savage et al., 2010) grown at HL, ML and LL. B, the carboxysome content within the *Synechococcus* cells is dependent on light intensity, in agreement with the observation of RbcL:eGFP and CcmK4:eGFP cells. Error bars represent SD (n = 250). Scale bar: 2 μm.

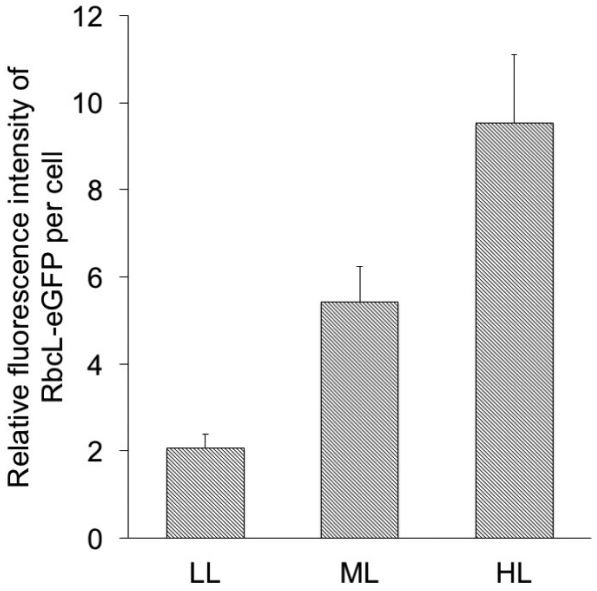

Supplemental Figure S6. Relative abundance of RuBisCO in RbcL:eGFP *Synechococcus* strain under LL, ML and HL, based on confocal image analysis. Analysis of the relative fluorescence intensity of RbcL:eGFP per cell based on confocal images (Fig. 2) exhibits the increase of GFP intensity in the *Synechococcus* cell with the rise of illumination intensity, indicating that stronger illumination could stimulate the biosynthesis of RuBisCO enzymes (n = 100). It is further confirmed by immunblot analysis shown in Fig. 4. Error bars represent SD.

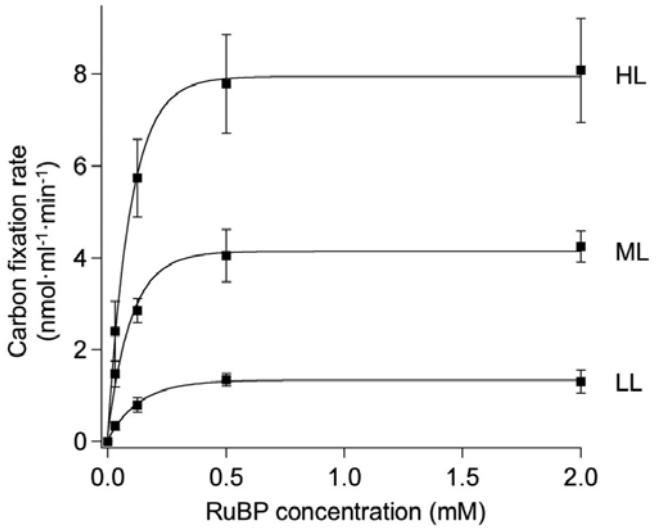

Supplemental Figure S7. ^{14}C carbon fixation rates of wild-type *Synechococcus* cells grown under LL, ML and HL, as a function of RuBP concentration (± SD, $n = 6$). The carbon fixation rate of wild-type cells in HL (7.8 μmol·min^{-1}·ml^{-1}) is higher compared with those in ML (4.0 μmol·min^{-1}·ml^{-1}) and LL (1.3 μmol·min^{-1}·ml^{-1}). The curves were fitted exponentially. The cell density was calibrated using the AtpB content of cells. 0.5 mM RuBP was used during RuBisCO assay in this study to determine the maximum carbon fixation rates (see Fig. 4).

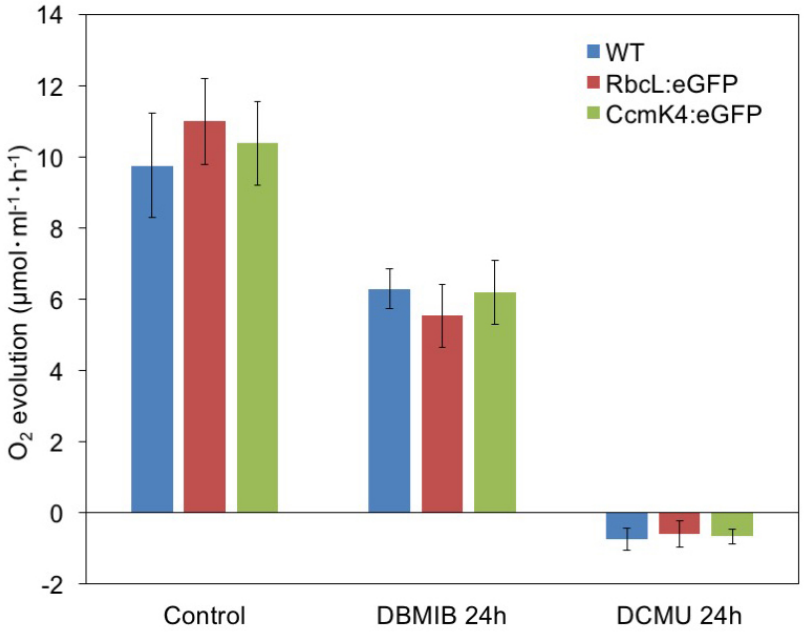

Supplemental Figure S8. Oxygen evolution analysis of *Synechococcus* cells in the presence of DBMIB and DCMU for 24 hours. Error bars represent SD (n = 4). The oxygen evolution was inhibited in the presence of DBMIB for 24 hours and was not detectable in the presence of DCMU.

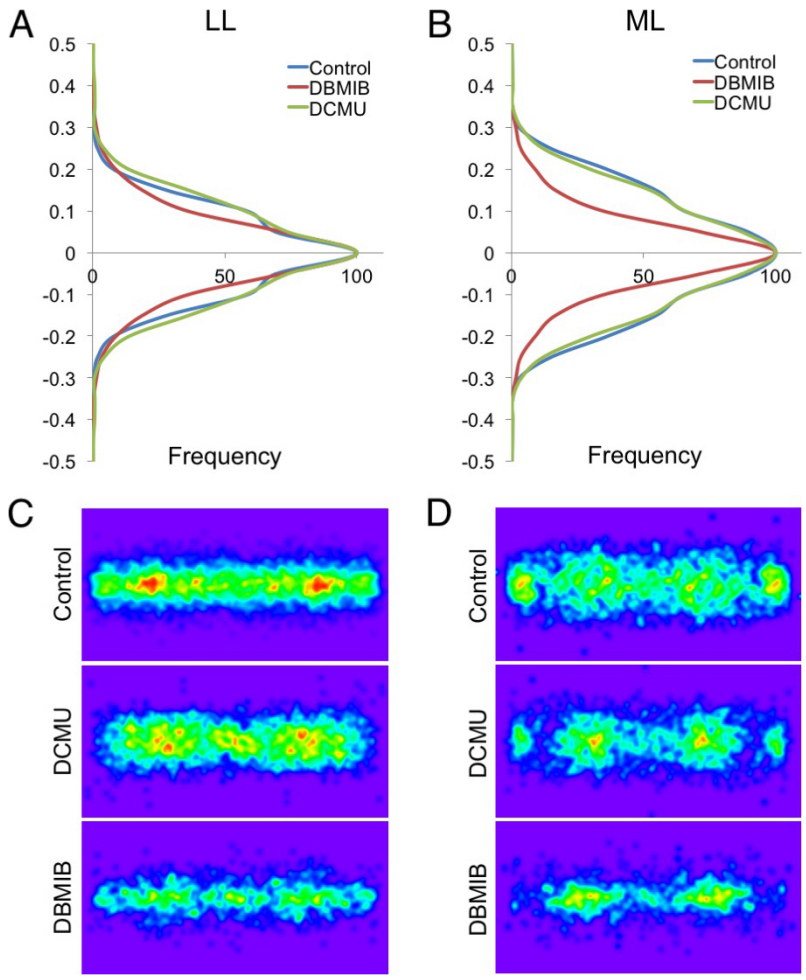

Supplemental Figure S9. Organization of carboxysomes in LL- and ML-adapted cells under the treatment of DCMU and DBMIB. A and B, The narrow distributions of carboxysomes along the short axis of LL- and ML-adapted cells under DBMIB treatment (n = 300), compared to the wider distribution induced by DCMU treatment, indicated the redox state of PQ pool plays an important role in regulating the carboxysome localization in cells (Fig. 6). C and D, Normalized spatial distribution maps of carboxysomes within LL- and ML-adapted cells under the treatment of DCMU and DBMIB.

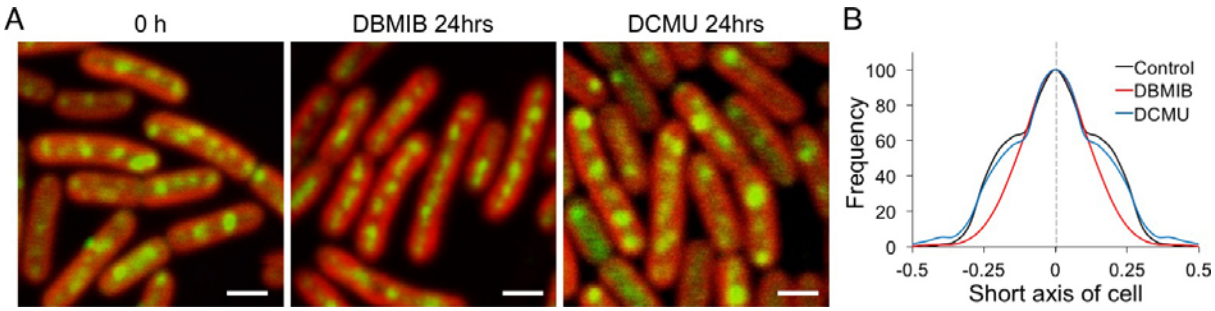

Supplemental Figure S10. The effects of DBMIB and DCMU on β-carboxysome localization in CcmK4:eGFP cells. **A,** Confocal images of HL-adapted CcmK4:eGFP cells under DBMIB and DCMU treatments for 24 hours. Scale bar: 1 μm. B, Analysis of carboxysome distribution along the short axis of cells (n = 200). It shows different effects of DBMIB and DCMU on the carboxysome positioning in *Synechococcus*, consistent with the observations of RbcL:eGFP cells.

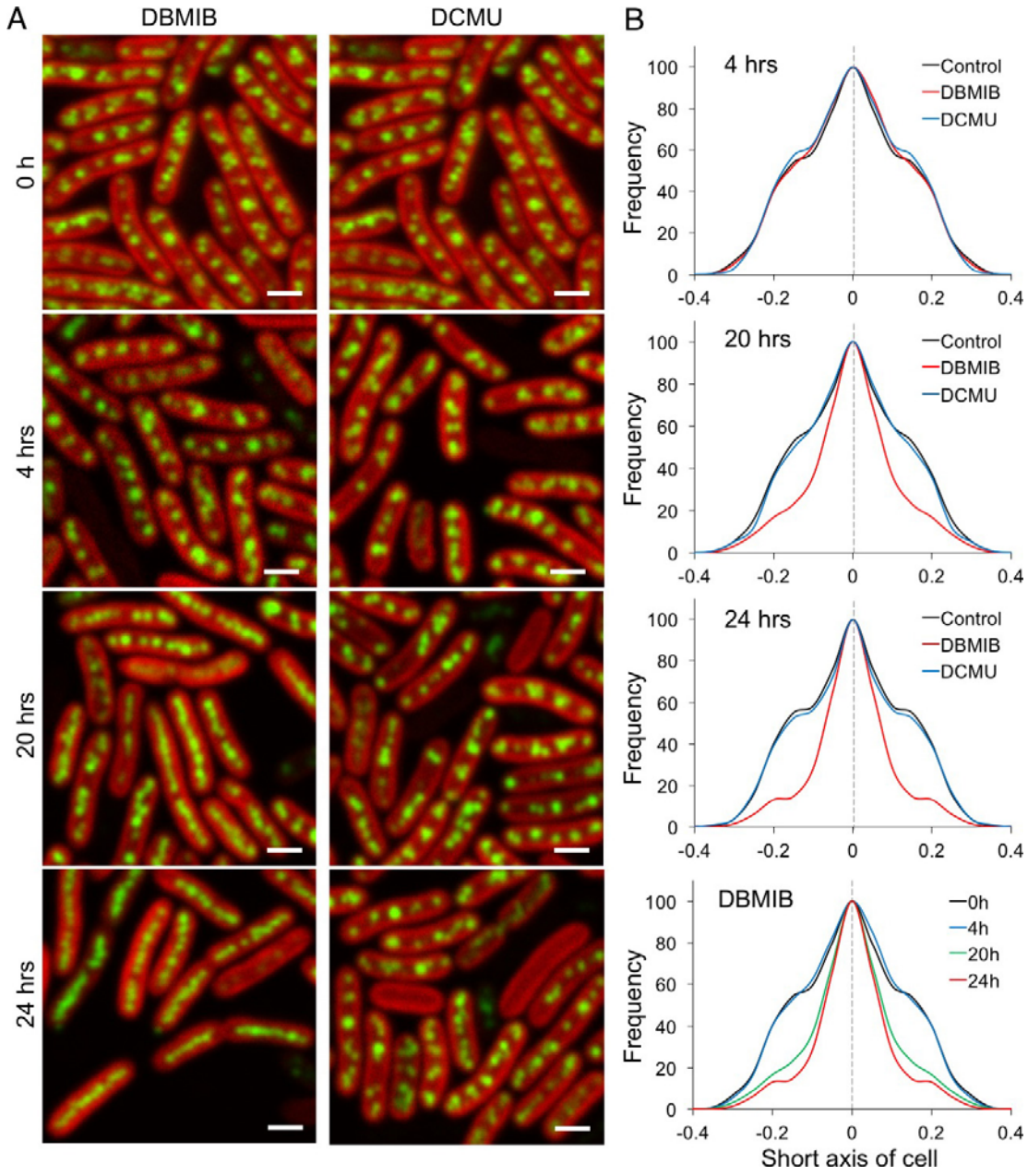

Supplemental Figure S11. Time-lapse confocal fluorescence imaging of RbcL:eGFP cells in the presence of DCMU and DBMIB. A, Confocal images of HL-adapted RbcL:eGFP cells with DBMIB and DCMU treatments for 4, 20 and 24 hours. Scale bar: 1 μm. B, Carboxysome localization along the short axis of *Synechococcus* cells, demonstrating different effects of DCMU and DBMIB on the spatial positioning of carboxysomes. 24-hour inhibitor treatments were applied to characterize the changes in the carboxysome distribution (see Fig. 6).